Science of the Total Environment 853 (2022) 158450

Contents lists available at ScienceDirect

Science of the Total Environment

journal homepage: www.elsevier.com/locate/scitotenv

Highly time-resolved measurements of elements in $PM_{2.5}$ in Changzhou, China: Temporal variation, source identification and health risks

Yanan Yi [a,b], Qing Li [a,b], Kun Zhang [a,b], Rui Li [a,b], Liumei Yang [a,b], Zhiqiang Liu [a,c], Xiaojuan Zhang [a,c], Shunyao Wang [a,b], Yangjun Wang [a,b], Hui Chen [a,b], Ling Huang [a,b], Jian Zhen Yu [d,e], Li Li [a,b,*]

[a] School of Environmental and Chemical Engineering, Shanghai University, Shanghai 200444, China
[b] Key Laboratory of Organic Compound Pollution Control Engineering (MOE), Shanghai University, Shanghai, China
[c] Jiangsu Changhuan Environment Technology Co., Ltd., Changzhou 213002, China
[d] Department of Chemistry, Hong Kong University of Science & Technology, Hong Kong, China
[e] Division of Environment & Sustainability, Hong Kong University of Science & Technology, Hong Kong, China

HIGHLIGHTS

- 19 elements in $PM_{2.5}$ in winter were measured in-situ in Changzhou.
- Iron and steel industry and soil dust were the predominant sources to elements in $PM_{2.5}$.
- Controlling emissions of Cr, Co and As could be an effective way to protect public health.

GRAPHICAL ABSTRACT

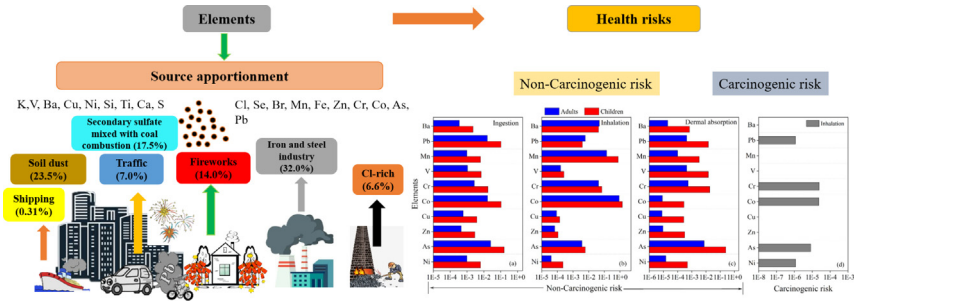

ARTICLE INFO

Editor: Hai Guo

Keywords:
Elements
Source apportionment
Health risks
$PM_{2.5}$

ABSTRACT

The temporal variation, sources, and health risks of elemental composition in fine particles ($PM_{2.5}$) were explored using online measurements of 19 elements with a time resolution of 1 h at an urban location in Changzhou, China, from December 10, 2020 to March 31, 2021. The mass concentration of $PM_{2.5}$ was 50.1 ± 32.6 μg m^{-3}, with a range of 3–218 μg m^{-3}. The total concentration of 19 elements (2568 ± 1839 ng m^{-3}) accounted for 5.1 % of $PM_{2.5}$ mass concentration. S, Cl, Si, and Fe were the dominant elementary species, accounting for 90 % of total element mass concentrations during the whole campaign. Positive matrix factorization (PMF) model was applied to identify the major emission sources of elements in $PM_{2.5}$. Seven factors, named secondary sulfate mixed with coal combustion, Cl-rich, traffic, iron and steel industry, soil dust, fireworks, and shipping, were identified. The major sources for elements were iron and steel industry, followed by soil dust and secondary sulfate mixed with coal combustion, explaining 32.0 %, 23.5 % and 16.7 % of the total source contribution, respectively. The total hazard index (HI) of elements was 3.01 for children and 1.18 for adults, much greater than the admissible level (HI = 1). The total carcinogenic risk (CR) in Changzhou was estimated to be 5.87 × 10^{-5}, which was above the acceptable CR level (1 × 10^{-6}). Among the calculated metal elements, Cr, Co and As have higher carcinogenic risk, and Co was found to trigger the highest noncarcinogenic risk to Children. Our results indicate that industrial emission is the dominant CR contributor, emphasizing the necessity for stringent regulation of industry sources. Overall, our study provides useful information for policymakers to reduce emissions and health risks from elements in the Yangtze River Delta region.

* Corresponding author at: School of Environmental and Chemical Engineering, Shanghai University, Shanghai 200444, China.
E-mail address: Lily@shu.edu.cn (L. Li).

http://dx.doi.org/10.1016/j.scitotenv.2022.158450
Received 11 June 2022; Received in revised form 28 August 2022; Accepted 28 August 2022
Available online 2 September 2022

1. Introduction

It is well known that ambient air pollution is one of the greatest public health hazards worldwide, given that it accounts for millions of premature deaths per year (WHO, 2022). Particulate matter (PM) has significant impact on air quality and human health (Chang et al., 2018; Cui et al., 2020a; Rai et al., 2020b). Numerous epidemiological surveys have discovered significant relationships between PM and adverse health influences over short or long term exposure events (Pope et al., 2018). Fine particulate matter ($PM_{2.5}$), with relatively small particle size, can float for a long time in the air before entering human body, resulting in aspiratory and cardiovascular illnesses, malignant tumor, as well as neural system and reproductive dysfunctions (Manisalidis et al., 2020; Pope et al., 2018).

Ambient trace elements account for a minor proportion of $PM_{2.5}$ mass concentration in urban atmosphere, while elemental components such as As, Co, Cr, Ni, Pb, Se, and Cd have been identified as human carcinogens (Chang et al., 2018). The major exposure methods of heavy elements in $PM_{2.5}$ are hand-mouth intake, inhalation, and dermal absorption (Xu et al., 2019). Metal elements enriched in $PM_{2.5}$ can penetrate human body and deposit in different ways, causing dysfunction and irreversible damage to the human body (Yan et al., 2022). Moreover, some elements (e.g., transition elements, Mn, Ti, Cu, Fe and V) also play important roles in catalyzing atmospheric photochemical oxidation process and further contribute to secondary aerosol formation (Deng et al., 2020; Li et al., 2017; Wang et al., 2021b). Therefore, it is necessary to access the chemical composition, sources and health risks of toxic elements in $PM_{2.5}$.

Source identification and quantification of elements are significant in investigating the relationship among source emissions, environmental concentrations, health impact and environmental influences (Rai et al., 2020a). Previous studies have indicated that elements can be used as markers to identify and potential sources of $PM_{2.5}$, particularly anthropogenic emissions (e.g., industrial, traffic, and coal combustion) in cities (Rai et al., 2021; Zhao et al., 2021). Compared to offline observation, high temporal resolution instrument can collect aerosol and analyze samples in real-time for long-term observations without laboratory analysis (Rai et al., 2020b). Online measurement can provide insights into real-time dynamic changes and primary local sources of $PM_{2.5}$-bound elements in urban areas. Such rapid changes and episodic events cannot be observed by conventional offline filter observations (using a 12 or 24 h time resolution) (Chang et al., 2018; Zhao et al., 2021). PMF model, as one of the receptor models, was widely used for source apportionment of trace elements. As of now, several studies by using high time resolution elemental data have identified different sources via PMF model, such as coal combustion, traffic, oil combustion, fireworks, industrial, road dust, secondary sulfate and metal smelting (Chang et al., 2018; Cui et al., 2020b; Rai et al., 2020a; Rai et al., 2020b; Reizer et al., 2021). Therefore, hourly measurement of ambient elements of $PM_{2.5}$ is important and necessary to understand their pollution levels, chemical constitutions, evaluate the variation features and identify the sources of trace elements.

Changzhou, one of the central cities in the Yangtze River Delta (YRD) region, China, and a typical city with dense population and heavy industry (Jensen et al., 2021), normally experiences heavy air pollution episodes, especially in winter. Previously, several studies of elements in $PM_{2.5}$ have been conducted in Changzhou (Liu et al., 2018b; Wang et al., 2015). However, there are few observations of elements in $PM_{2.5}$ with high time resolution, leading to unclear pollution formation and source identification. Therefore, in order to understand the characteristics of pollution and sources of $PM_{2.5}$-bound elements in a typical city of China, it is essential to perform high time resolution measurements to obtain the pollution formation processes and sources in time, providing scientific evidence for better air pollution control strategies. 19 elements in $PM_{2.5}$ in urban Changzhou were observed in this study with 1-h time-resolution from December 10, 2020 to March 31, 2021. The major purposes of this study are: (1) study the chemical composition, concentration and temporal variation of elements in $PM_{2.5}$; (2) identify the sources of elements via enrichment factor and PMF model; (3) determine the health risk of the elements in $PM_{2.5}$; (4) compare the concentration of each element and source contribution to total elements during different pollution episodes. Results of this study could be beneficial to the development of control strategies tackling air pollution in the YRD region.

2. Methodology

2.1. Observational site

In this study, hourly observations of $PM_{2.5}$-bound elements were conducted on the rooftop of Changzhou Environmental Monitoring Center (31°45′ N, 119°57′ E), Jiangsu Province, China (Fig. 1a–d). Fig. 1a shows a map of China's provincial borders, in which Jiangsu Province is located in the eastern coast of China (Fig. 1b). Fig. 1c and d show the sampling site and a detailed map of the surrounding environment. It can be seen that the sampling site were surrounded by residential areas, business streets and traffic roads (such as Guanghua Road, Heping Road, Zhongwu Avenue and Jingling South Road) without obvious industrial sources (Fig. 1d).

2.2. Field campaign

Ambient mass concentrations of elements in $PM_{2.5}$ were detected with an atmospheric heavy metal on-line analyzer (EHM-X 200, Skyray, China) by using X-ray fluorescence (XRF). 19 elements (K, Ni, Si, S, Cl, Br, Se, As, Zn, Cu, Co, Cr, V, Ti, Ca, Mn, Fe, Pb, and Ba) were measured with 1 h time resolution. $PM_{2.5}$ mass concentrations were detected at 1 h time resolution by using β-ray technology from Continuous Particulate Matter Monitor (BAM1020, Met One Inc., US). Meteorological parameters, including temperature (T), relative humidity (RH), wind speed (WS) and wind direction (WD), were obtained by a weather transmitter (WXT520, Vaisala Inc., Finland), which uses ultrasonic to measure wind speed and wind direction, and the PTU module (a pronoun for the built-in module of the weather transmitter) uses oscillating and capacitive measurement method to measure atmospheric pressure, temperature, and humidity. Quality assurance and quality control (QA/QC) for the elements data was implemented during the whole sampling period, and the deviations between the measured concentration and standard concentration for individual elements were <5 %. The internal quality control checks of samples were conducted for 30 min every day during the sampling period. In addition, the stability of the instrument measurement was ensured by measuring the Pb rob inside the instrument. The minimum detection limits (1 h resolution, ng m^{-3}) during the measurement were: K (1.51), Ni (0.10), Si (14.9), S (5.8), Cl (3.2), Br (0.23), Se (0.16), As (0.12), Zn (0.29), Cu (0.33), Co (0.30), Cr (0.12), V (0.13), Ti (0.28), Ca (0.33), Mn (0.10), Fe (0.24), Pb (0.17), and Ba (0.43).

2.3. Enrichment factors

The natural or anthropogenic sources of elements were determined by the enrichment factors (EFs). The EFs of element in this work were calculated by Eq. (1).

$$EF_i = \frac{(C_i/C_{Si})_{aerosol}}{(C_i/C_{Si})_{crust}} \quad (1)$$

where $(C_i/C_{Si})_{aerosol}$ stands for the concentration ratio of element *i* and Si in aerosol samples, and $(C_i/C_{Si})_{crust}$ stands for the concentration ratio of element *i* and Si in the upper continental crust (Ministry of Environmental Protection of the People's Republic of China (MEP), 1990). Si was used as the reference element in this study due to its relative stability in the environment. Table S1 presented the concentration of elements in the upper continental crust in Jiangsu Province. EF_i value close to 1 suggest that the element *i* is emitted from the natural sources, while the $EF_i < 10$ means the impact of crustal sources (e.g., soil dust) on the element *i* is predominant. Additionally, anthropogenic sources are predominant when the EF_i is higher than 10 (Ellouz et al., 2013).

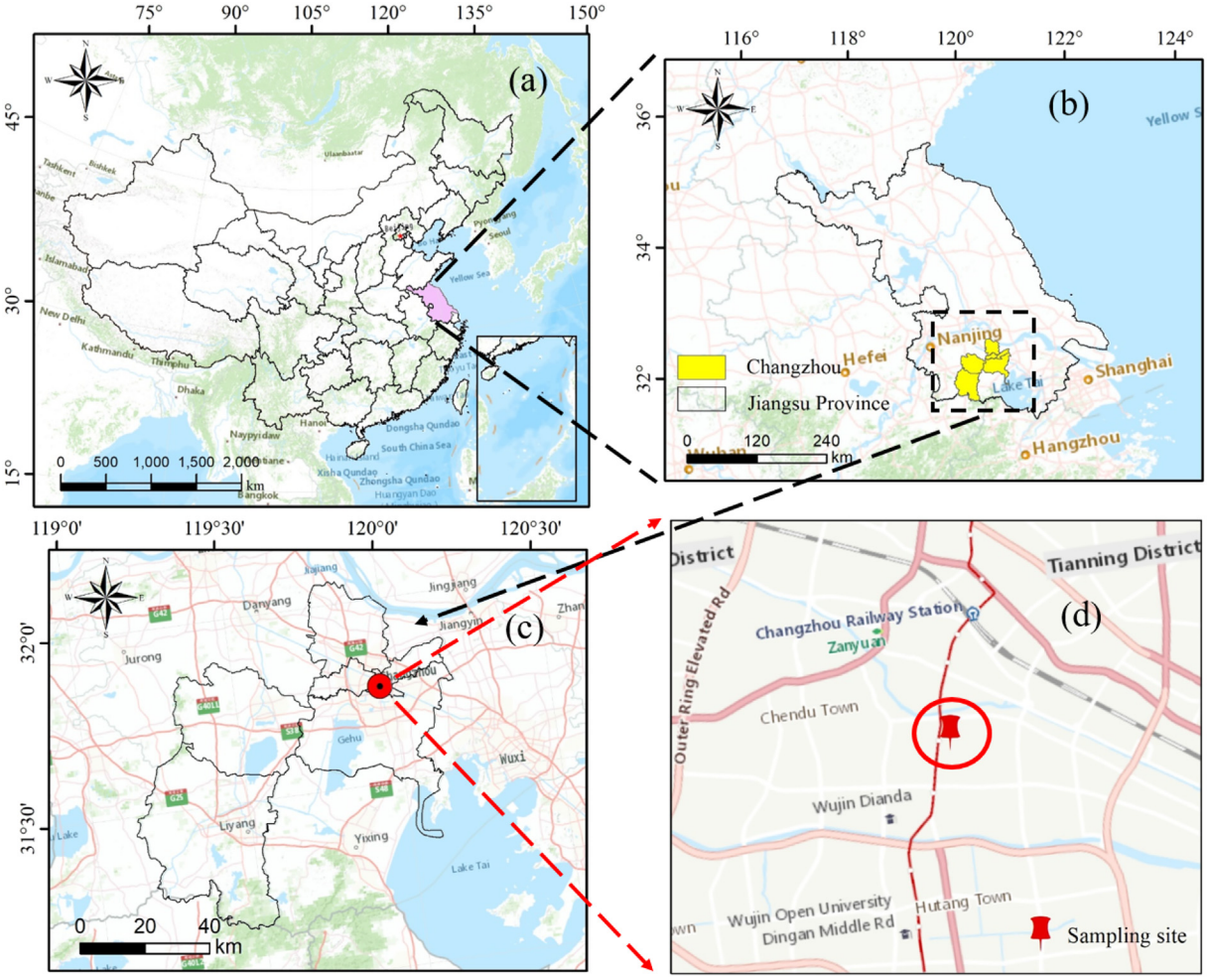

Fig. 1. Location map of the sampling site.

2.4. Positive matrix factorization model

PMF model, as a multivariate factor analysis receptor model, was extensively used for identifying and quantifying the major emission sources of elements in previous studies (Cui et al., 2020b; Li et al., 2022; Shukla et al., 2021; Zhang et al., 2018). In brief, source factor contributions were calculated with application of PMF model using a weighted least square fit method. The details of PMF have been summarized in previous studies (Manousakas et al., 2017; Paatero and Tapper, 1994; Reizer et al., 2021). In this study, the US Environmental Protection Agency (EPA) PMF 5.0 was used to ascribe elements to particular sources.

Here, three to nine factors solutions were initially tested to obtain the ideal factor based on the change of Q_{true}/Q_{exp}, and then the ideal factors were distinguished for more detailed PMF source analysis. As shown in Fig. S1, the ratios of Q_{true}/Q_{exp} were decreased from 6.96 to 3.37 when the factorization increased from three to nine. The decrease of Q_{true}/Q_{exp} ratio was smaller for six moving to seven factors compared to seven moving to eight factors, as is shown in Fig.S1. Therefore, the most reliable solution of seven factors was based on the variation of Q_{true}/Q_{exp} and the interpretability of the results.

2.5. Health risk assessment

Heavy metals can cause health problems through ingestion (ing), inhalation (inh), and dermal absorption (derm) (Zheng et al., 2010). Based on the method of US EPA, Integrated Risk Information Database and the International Agency for Research on Cancer, the elements can be divided into two different types (noncarcinogenic and carcinogenic). Among the measured elements in this study, Ni, As, Zn, Cu, Co, Cr, V, Mn, Pb and Ba were identified as noncarcinogenic species, and Ni, As, Co, Cr and Pb were regarded as carcinogenic species.

For the noncarcinogenic risk (NCR), the exposure level of $PM_{2.5}$-bound metals was evaluated by computing the average daily dose (ADD) for ingestion (ing), inhalation (inh), and dermal absorption (derm).

$$ADD_{ing} = \frac{C \times IngR \times EF \times ED}{AT \times BW} \quad (2)$$

$$ADD_{inh} = \frac{C \times InhR \times EF \times ED}{AT \times BW} \quad (3)$$

$$ADD_{derm} = \frac{C \times SL \times SA \times ABS \times EF \times ED}{AT \times BW} \quad (4)$$

$$HQ = \frac{ADD}{RfD} \quad (5)$$

where C is the concentration (mg m^{-3} for inhalation or mg kg^{-1} for ingestion and dermal absorption) of metals; IngR and InhR refers to ingestion rate (children: 100 mg day^{-1}; adults: 200 mg day^{-1}) and inhalation rate (7.5 m^3 day^{-1} for children and 15 m^3 day^{-1} for adults) (EPA, 2011; Yan et al., 2022). EF refers to exposure frequency (days $year^{-1}$); ED is the expose duration (for children: 6 years; for adults: 24 years); AT is the average exposure time (for noncarcinogenics: AT = ED × 365 days; for carcinogenic, AT = 70 years × 365 days) (Zhang et al., 2018); BW is the mean body weight (kg) (MEP. Ministry of Environmental Protection of the

People's Republic of China (MEP), 2019); SL and SA refer to skin adherence factor (0.2 mg m^{-2} day^{-1} for children and 0.07 mg m^{-2} day^{-1} for adults) and skin surface area (2800 cm^2 for children and 5700 cm^2 for adults), respectively. ABS is the skin absorption coefficient (0.03 As and 0.001 for other metals). RfD is a receivable risk value for metal (Table S2); HQ is the hazard quotient, and the hazard index (HI) was then computed by adding all metals along with noncarcinogenic impacts. Values of HQ or HI higher than 1 indicate a significant unfavorable noncarcinogenic effect of lifetime of exposure in children and adults.

For the carcinogenic risk (CR), the inhalation exposure route of carcinogenic elements was evaluated by figuring out the lifetime average daily dose (LADD) for inhalation (inh). The calculation formula is as follows (Alharbi et al., 2019; Kong et al., 2015; Wang et al., 2021a):

$$LADD_{inh} = \frac{C \times EF}{AT} \times \left(\frac{InhR_{child} ED_{child}}{BW_{child}} + \frac{InhR_{adult} ED_{adult}}{BW_{adult}} \right) \quad (6)$$

In this study, $LADD_{InhR}$ was calculated by adding time-weighted exposure in infancy and adulthood. AT refers to 70 × 365 days (Fan et al., 2021). The CR for metals was calculated by Eq. (7).

$$CR = LADD \times SF \quad (7)$$

where SF refers to the slope factor (mg (kg day)$^{-1}$, Table S2). The CR is calculated from the inhalation route in this study owing to the lack of SF for ingestion or dermal absorption (Yan et al., 2022). When CR is equal to 10^{-6}, the risk is receivable, while a CR value above 10^{-4} means significant cancer risk. All relevant parameters used in NCR and CR have been documented in Table S2 and Table S3.

3. Results and discussion

3.1. Overview of field measurements

The meteorological conditions, ambient concentrations of $PM_{2.5}$ and elements are summarized in Table 1 and Fig. 2. During the field campaign, the hourly temperature (T) varied from −7.3 °C to 27.7 °C with an average of 9.3 ± 5.5 °C; the relative humidity (RH) ranged from 15 % to 85 % with an average of 54.2 ± 17.8 %. The wind speed (WS) averaged at 1.4 ± 0.7 m/s with a range of 0.2–5 m/s. The precipitation ranged from 0.1 to 5.9 mm with an average of 0.69 mm. The total measured $PM_{2.5}$ mass concentrations at Changzhou was 50.1 ± 32.6 μg m^{-3} (ranged between 3 and 218 μg m^{-3}), which was about 3.3 times higher than the daily standard value (15 μg m^{-3}) advised by the World Health Organization (WHO, 2021). The mass concentration of $PM_{2.5}$ in non-precipitation days (50.9 ± 32.7 μg m^{-3}) was about 1.2 times higher than that on precipitation days (41.3 ± 30.1 μg m^{-3}), and the lowest concentration (3 μg m^{-3}) appeared on precipitation days (Fig. 2), indicating that wet deposition play an important role in removing $PM_{2.5}$ (Zhang et al., 2019). Compared to other cities in winter, the $PM_{2.5}$ concentrations observed in Changzhou was lower than that in northern China (Cui et al., 2020b), such as Tianjin (67 ± 64 μg m^{-3}), Shijiazhuang (83 ± 65 μg m^{-3}), and Zhengzhou (70 ± 50 μg m^{-3}), but higher than that measured in Shanghai (46 ± 34 μg m^{-3}) (Li et al., 2020), Nanjing (45.5 μg m^{-3}) (Cao et al., 2021) and Guangzhou (40.2 ± 19.3) (Huang et al., 2022). The above results indicate that the $PM_{2.5}$ pollution in Changzhou in winter is significant. As shown in Fig. 2, the maximum daily mean $PM_{2.5}$ value (141 μg m^{-3}) at Changzhou was observed on 12 December 2020, which was about 9.4 times higher than the daily air quality standard (15 μg m^{-3}) defined by WHO. In this study, nine pollution episodes (marked as P1–P9), with 1 Chinese New Year period (CNY) and 1 dust period (Dust) were identified and highlighted in Fig. 2, with pollution episodes in gray, CNY in pink and dust in yellow. According to the Ambient Air Quality Standards of China (GB 3095–2012), the daily $PM_{2.5}$ for the 1st and 2nd standard values are 35 μg m^{-3} and 75 μg m^{-3}, respectively. Therefore, the nine pollution episodes in this study were named when the daily average $PM_{2.5}$ concentration

Table 1
Differences in meteorological factors, elements (ng m^{-3}) and $PM_{2.5}$ (μg m^{-3}) concentrations during the pollution episodes (P1-P9), Chinese New Year (CNY), Dust and whole periods in Changzhou.

Species	Whole period	P1	P2	P3	P4	P5	P6	P7	P8	P9	CNY	Dust
$PM_{2.5}$	50.1 ± 32.6	113 ± 45.6	98.4 ± 24.5	100 ± 36	85.8 ± 20.8	79.3 ± 34.9	92.3 ± 11.1	75.4 ± 18.4	78.9 ± 15.9	95.6 ± 30.9	35.8 ± 14.8	65.0 ± 14.1
RH (%)	54.2 ± 17.8	63.6 ± 10.2	49.5 ± 12.9	62 ± 11.4	43.3 ± 13.4	76.4 ± 3.4	66.3 ± 3.7	58.2 ± 15.2	63.6 ± 7.2	63.4 ± 12.8	57.9 ± 14.9	58.4 ± 19.2
WS (m/s)	1.4 ± 0.7	0.8 ± 0.5	0.8 ± 0.3	0.8 ± 0.5	1.5 ± 1.0	0.7 ± 0.3	1.3 ± 0.4	1.3 ± 0.6	1.6 ± 0.4	1.3 ± 0.5	1.3 ± 0.6	2.7 ± 0.4
T (°C)	9.3 ± 5.5	8.5 ± 2.1	7.3 ± 3.1	11.0 ± 2.5	10.7 ± 4.3	12.3 ± 0.8	6.9 ± 1.7	7.6 ± 1.9	11.5 ± 1.6	15.1 ± 3.2	10.9 ± 3.9	16.1 ± 2.2
K	267 ± 396	271 ± 141	357 ± 163	343 ± 173	251 ± 78.5	159 ± 114	207 ± 114	116 ± 74.6	141 ± 88.6	155 ± 98.7	1043 ± 1136	646 ± 518
Ni	12.7 ± 7.7	14.0 ± 8.1	17.4 ± 8.7	16.5 ± 7.7	10.0 ± 5.9	12.3 ± 7.0	12.4 ± 7.2	11.7 ± 7.7	18.0 ± 7.0	17.0 ± 8.6	11.3 ± 6.2	19.3 ± 10.1
Si	345 ± 776	173 ± 99.3	254 ± 104	287 ± 105	388 ± 273	168 ± 74.4	200 ± 81.9	288 ± 317	261 ± 99.9	282 ± 93.0	117 ± 86.0	4218 ± 3746
S	810 ± 768	1798 ± 1081	725 ± 475	830 ± 522	357 ± 401	742 ± 519	2335 ± 445	1431 ± 769	816 ± 460	1336 ± 382	1404 ± 907	810 ± 810
Cl	467 ± 532	645 ± 456	1359 ± 1134	1110 ± 1150	455 ± 278	677 ± 349	562 ± 418	171 ± 127	424 ± 362	289 ± 254	454 ± 494	88.6 ± 88.8
Br	6.7 ± 6.7	8.4 ± 4.9	13.7 ± 7.3	11.5 ± 5.9	10.1 ± 7.8	12.0 ± 5.2	6.9 ± 6.4	6.3 ± 6.4	5.8 ± 3.6	8.9 ± 8.1	4.9 ± 3.3	4.0 ± 3.9
Se	3.7 ± 2.5	4.2 ± 2.4	4.4 ± 2.4	5.3 ± 3.0	4.4 ± 2.3	3.4 ± 1.7	3.8 ± 2.6	4.0 ± 2.5	5.1 ± 2.9	3.8 ± 2.2	3.8 ± 2.4	3.1 ± 2.3
As	5.3 ± 4.9	5.4 ± 4.0	8.1 ± 5.6	5.7 ± 4.0	5.9 ± 5.0	11.1 ± 16.2	4.9 ± 3.4	5.3 ± 3.9	4.2 ± 3.0	5.5 ± 3.9	4.2 ± 3.0	5.0 ± 3.6
Zn	88.9 ± 126	161 ± 110	216 ± 139	202 ± 156	96.5 ± 47.5	123 ± 44.9	112 ± 51.7	72.4 ± 78.1	154 ± 70.2	100 ± 70.2	29.3 ± 22.1	68.6 ± 39.8
Cu	15.5 ± 20.1	11.3 ± 10.6	26.2 ± 15.9	21.9 ± 26.2	24.6 ± 18.4	19.7 ± 12.6	11.2 ± 10.7	6.8 ± 5.0	26.2 ± 19.1	24.5 ± 29.2	30 ± 32.1	9.4 ± 14.1
Co	21.4 ± 15.9	30.2 ± 13.9	39.7 ± 16.5	37.7 ± 15.9	21.7 ± 6.9	24.9 ± 8.5	27 ± 14.6	18.5 ± 6.9	37.3 ± 12.8	31.2 ± 24.8	11.7 ± 5.1	68.0 ± 51.7
Cr	5.7 ± 6.5	7.6 ± 5.3	11.6 ± 8.7	12.0 ± 8.5	4.1 ± 2.5	6.3 ± 4.3	9.5 ± 7.7	2.9 ± 2.3	11.2 ± 5.4	7.9 ± 6.0	2.5 ± 2.0	5.1 ± 4.4
V	5.0 ± 6.2	4.0 ± 2.2	4.8 ± 2.1	5.4 ± 2.7	4.5 ± 1.9	4.5 ± 2.1	4.1 ± 2.5	3.1 ± 1.6	4.2 ± 1.9	4.8 ± 2.4	15.5 ± 16.1	18.6 ± 15.0
Ti	10.9 ± 19.6	6.8 ± 4.8	9.0 ± 7.0	11.6 ± 8.3	6.9 ± 6.0	3.2 ± 2.9	7.4 ± 5.6	8.1 ± 7.2	10.2 ± 6.6	8.0 ± 7.3	5.3 ± 4.7	112.4 ± 98.0
Ca	103 ± 105	70.3 ± 49.3	158 ± 83.3	129 ± 91.3	165 ± 119	47.4 ± 42.2	77.9 ± 49.7	132 ± 150	102 ± 57.7	79.5 ± 49.0	32.1 ± 26.1	426 ± 359
Mn	29.4 ± 23.3	49.5 ± 24.5	70.1 ± 31.0	60.7 ± 31.9	30.6 ± 11.6	40.2 ± 15.3	37.6 ± 21.4	20.0 ± 6.7	55.4 ± 20.3	48.9 ± 33.3	12.9 ± 8.6	53.3 ± 31.6
Fe	321 ± 292	482 ± 254	669 ± 288	627 ± 283	327 ± 85.8	395 ± 146	402 ± 253	266 ± 113	627 ± 246	48.0 ± 320.	133 ± 84.2	1253 ± 1011
Pb	37.2 ± 32.4	40.0 ± 18.5	64.0 ± 31.0	40.2 ± 19.9	32.5 ± 18.3	48.2 ± 32.3	62.1 ± 41.4	31.0 ± 18.6	35.3 ± 16.5	32.0 ± 17.7	44.0 ± 36.5	31.5 ± 30.9
Ba	18.3 ± 38.9	10.1 ± 7.2	12.0 ± 8.4	14.0 ± 9.1	9.3 ± 5.4	9.8 ± 5.7	8.3 ± 7.6	5.8 ± 4.3	10.9 ± 8.2	9.6 ± 7.7	95.8 ± 124	28.0 ± 21.2
Total elements	2568 ± 1839	3792 ± 2297	4019 ± 2530	3770 ± 2623	2204 ± 1375	2508 ± 1403	4091 ± 1544	2600 ± 1702.5	2747 ± 1492	2931 ± 1418	3454 ± 2998	7867 ± 5537

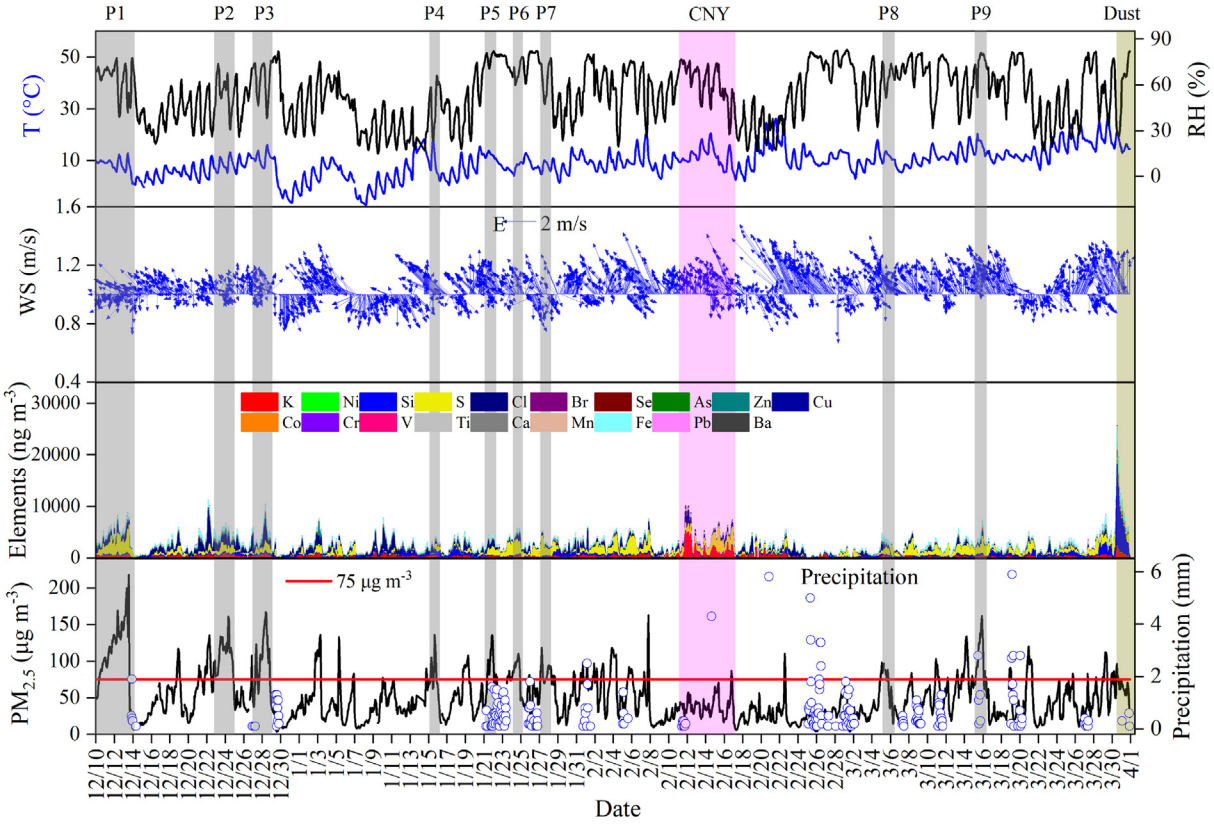

Fig. 2. Temporal variations of meteorological parameters (WS, m/s; T, °C; RH, %; Precipitation, mm), concentrations of elements (ng m^{-3}) and $PM_{2.5}$ (μg m^{-3}) in Changzhou during the field campaign.

was higher than 75 μg m^{-3}. Table 1 and Fig. S2 shows that the prevailing wind during pollution episodes was from the southeast. Calm conditions (~1 m/s) and high humidity (> 60 %) were frequently found during the P1 P2 and P9, which suggested that high RH and calm weather contribute to the accumulation of pollutants and then cause the formation of haze (Fan et al., 2021). $PM_{2.5}$ concentrations (35.8 μg m^{-3}) during the Chinese New Year was close to China's 1st standard limit (35 μg m^{-3}, GB 3095–2012).

The hourly mean values of total elements were 2568 ± 1839 ng m^{-3} at Changzhou during the campaign (Table 1), accounting for 5.1 % of $PM_{2.5}$ (50.1 ± 32.6 μg m^{-3}). Compared to other studies (Table S4), most elements in Changzhou were found to be much lower than those observed in Beijing (Fan et al., 2021), Nanjing (Yu et al., 2019), and Delhi, India (Rai et al., 2020a), but higher than what were measured in Shanghai, China (Cheng et al., 2022) and Warsaw, Poland (Reizer et al., 2021). Concentrations of Zn, Cr, Mn and Fe in this study are higher than Shanghai, which may be related to the existence of denser iron and steel industries in Changzhou.

In general, S was found to be the most abundant elements with an average concentration of 810 ± 768 ng m^{-3}, followed by Cl (467 ± 532 ng m^{-3}), Si (345 ± 776 ng m^{-3}), Fe (321 ± 292 ng m^{-3}), K (267 ± 396 ng m^{-3}) and Ca (103 ± 105 ng m^{-3}), and the sum of above elements accounted for 90 % of total elements concentration (Table 1). The concentrations of Zn, Pb, Mn, Co, Ba, Cu, Ni and Ti were at a range of 10–100 ng m^{-3}, but Br, Cr, As, V, and Se were <10 ng m^{-3}. Previous studies have indicated that high contents of K, V, Ba and Cu are related to fireworks and firecrackers burning (Kong et al., 2015; Tian et al., 2014). As can be seen from Fig. 2, some peaks of elements occurred during the whole sampling period, the peaks of K, Cu, V and Ba concentrations were observed from February 11 to February 17, 2021 (CNY period), with hourly peak values of these elements reaching up to 5259 ng m^{-3}, 169 ng m^{-3} and 709 ng m^{-3}, respectively. Therefore, all those peak values of elements could be attributed to the intensive fireworks during the Chinese Lunar New Year (Cui et al., 2020a). Furthermore, high values of Si, Ti, Ca and Fe were observed in late spring and were related to the dust storm. During the dust storm episode on March 30–31, 2021, the peak values of Si, Ti, Ca and Fe elements reached 15,891 ng m^{-3}, 414 ng m^{-3}, 1506 ng m^{-3}, and 4491 ng m^{-3}, respectively. It is well known that short-term or prolonged exposure to these elements at high mass concentrations may increase the risk of acute or chronic disease among local populations (Pope et al., 2018; Zhou et al., 2018).

According to China's ambient air quality guidelines (GB 3095–2012) and the atmospheric mass concentrations limits of WHO, the threshold of value of Ni, As, Cr, V and Mn are 20 (25 for WHO), 6 (6.6 for WHO), 0.025 (0.25 for WHO), 1000 (WHO) and 150 (WHO) ng m^{-3}, respectively. In this study, the average concentrations of Cr (5.7 ± 6.5 ng m^{-3}) was higher than the limitation values of NAAQS and WHO, while the levels of other airborne metals in Changzhou were lower than the limits of China and WHO. It can be seen that there is heavy Cr pollution in Changzhou, which is likely to be affected by the local iron and steel industry.

3.2. Diurnal variations of elements

The hourly observation of $PM_{2.5}$-bound elements provides data to track the diurnal process of $PM_{2.5}$ sources and the generation of secondary aerosol in detail. Fig. 3 presents the diurnal variations of elements in $PM_{2.5}$ in Changzhou during the whole observational period. In this study, 7:00–19:00 is defined as daytime, and 20:00–6:00 is nighttime. Concentrations of K, V and Ba reflected the impact of fireworks. As shown in Fig. 3, the peak concentrations of K, Cu, V and Ba from 19:00 to 22:00 reflected the common sources caused by the burning of fireworks and firecrackers. Peak concentrations of Si, Ti and Ca were obviously higher in daytime than that in nighttime, which could be owing to anthropogenic activities, such as road dust. Concentrations of these elements decreased obviously in nighttime, which is possibly attributable to the road sweeping and

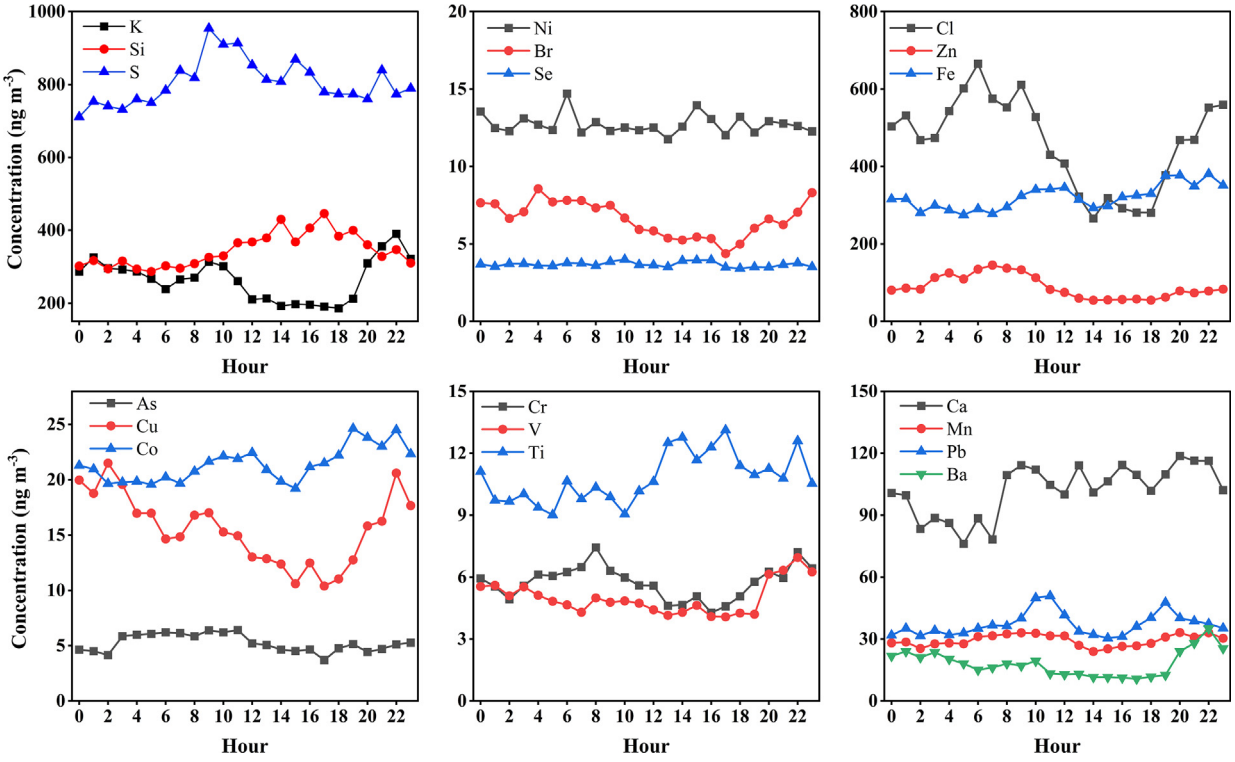

Fig. 3. Diurnal variations of elements in $PM_{2.5}$-bound elements.

watering work. As an abundant element species, S concentrations varied obviously throughout the daytime (Fig. 3), with lower concentrations during the nighttime, which reflected the influence of fossil fuel combustion or secondary formation. The two peak concentrations of Fe, Cu, Mn and Pb in the morning and evening demonstrated the effect of traffic during rush hours. Concentrations of K, Br, Cl, Fe, Cu V and Ba at nighttime were higher than those in daytime. Diurnal variation of Br, Cu, Cr, Mn and Fe is a good indication for the influences from industrial emissions and planetary boundary layer (PBL) changes. As shown in Fig. 3, the lowest concentrations of most elements occurred between 12:00 and 17:00, when the height of PBL and ambient temperature (Fig. S3) are both the highest during the daytime (Yu et al., 2019; Zhang and Cao, 2015).

3.3. Source identification and apportionment of $PM_{2.5}$-bound elements

3.3.1. Enrichment factors-based source identification

The EFs of elements in Changzhou during the campaign were presented in Fig. 4. The EFs of Ti and Ca were generally lower than 10, indicating that they were largely derived from crustal sources like soil suspended and dust storm. K and Fe were moderately enriched (10 < EFs < 100), indicating that they were largely influenced by anthropogenic sources (Yu et al., 2019). The EFs of Ni, Cl, Br, Se, As, Zn, Cu, Co, Cr, V, Mn, Pb and Ba were higher than 100, suggesting the dominant influences of human activities, such as industrial emissions, fossil fuel combustion, and traffic emissions (Jena and Singh, 2017; Xu et al., 2019).

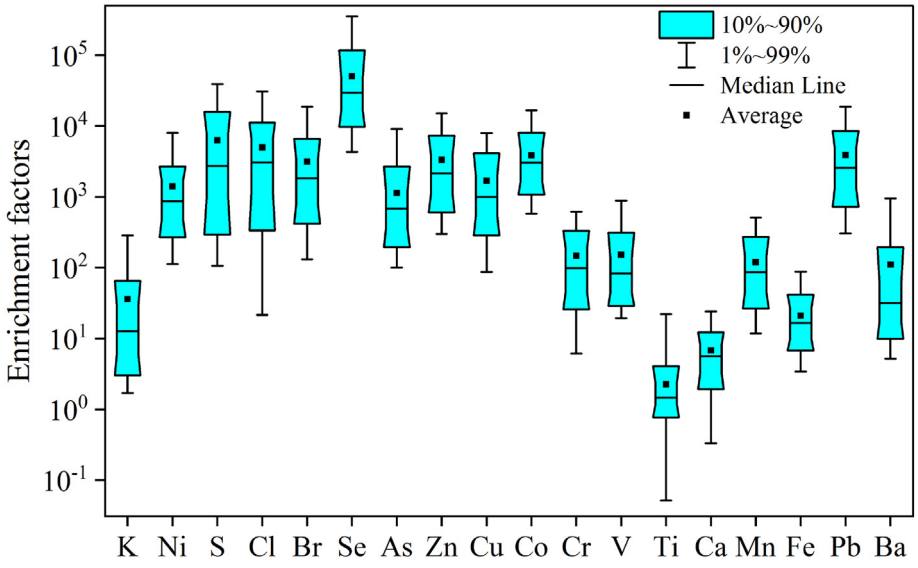

Fig. 4. Average enrichment factors of elements in Changzhou.

3.3.2. PMF-based source apportionment

In the PMF analysis, seven sources were figured out, including (1) secondary sulfate mixed with coal combustion, (2) Cl-rich, (3) traffic, (4) iron and steel industry, (5) soil dust, (6) fireworks, and (7) shipping. The profiles and contributions of seven PMF factors are shown in Fig. 5.

Factor 1 is characterized by the highest contribution of S (93.4 %). The abundance of S is likely related to a secondary product formed during the burning of sulfur-bearing fuels (Reizer et al., 2021). As shown in Fig. S4, S shows a significant correlation with SO_4^{2-} ($R^2 = 0.63$), which suggested that S is related to primary emissions and secondary formation from coal combustion, similar to many previous researches on source apportionment (Rai et al., 2020b; Reizer et al., 2021; Sharma et al., 2014). Therefore, the most likely source in this study is coal combustion, releasing large amount of SO_2, which in turn generates sulfate via oxidation. Furthermore, As also has a high loading (80.9 %) in factor 1. Studies have shown that As can be used as a reliable tracers for coal combustion (Cui et al., 2019; Reizer et al., 2021). Therefore, factor 1 can be attributed to the mixed source of secondary sulfate and coal combustion. The average relative contribution of secondary sulfate mixed with coal combustion factor to the analyzed elements mass was 16.7 %.

Factor 2 is mainly composed of high loadings of Cl (89.1 %) and Br (43.6 %), which is considered as a source of Cl-rich. Researches showed that Cl can be regarded as a tracer of coal combustion and biomass burning (Rai et al., 2021; Shukla et al., 2021; Zhang et al., 2018). In addition, anthropogenic Cl emissions are mainly in the form of HCl, which can be produced in the steel sector during the production of carbon steel products (Shukla et al., 2021). There are many iron and steel industries in Changzhou. In addition, the combustion of coal, garbage and biomass burning can also release HCl (Gani et al., 2019). Factor 2 shows increased concentrations from midnight until 9:00 (Fig. S6 (a)), largely influenced by the high RH, low temperature and low PBL during winter (Pant et al., 2015). Therefore, factor 2 can be considered as Cl-rich. The above evidence suggests that the Cl-rich factor is likely affected by steel industry, coal/garbage combustion and biomass burning. The contribution of Cl-rich factor to the overall analyzed elements mass was 6.6 %.

The most abundant elements in Factor 3 were Cu (78.8 %) and Pb (81.8 %). Cu is usually utilized as a lubricant and attrition material for the tyre or brake rotor (Lin et al., 2015), while Pb is associated with traffic emissions and can be discharged when the engine and brakes wear out (Han et al., 2015; Niu et al., 2021; Wang et al., 2016). The diurnal variations of Cu, Pb and PMF-derived elemental concentration for factor 3 shows an obvious morning peak and an evening peak (Fig. 3 and Fig. S6 (b)), and further indicates the reasonability of this source identification. Thus, factor 3 can be considered as a source of traffic, which explained 7.0 % of the analyzed elements and suggested emissions from traffic sources.

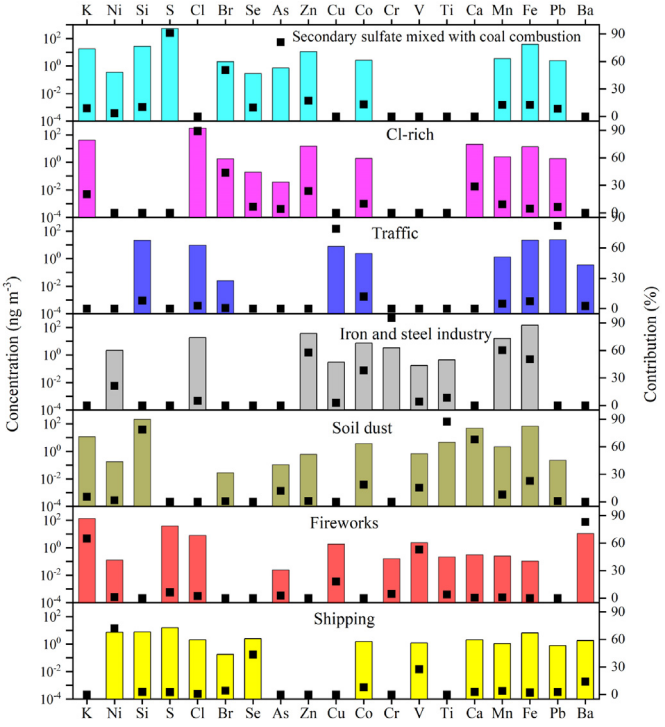

Fig. 5. Profiles and contributions of PMF factor identified for $PM_{2.5}$ in Changzhou.

The dominant elements in Factor 4 were Cr (95.4 %), Zn (57.8 %), Mn (60.2 %), Fe (50.4 %), and Co (38.3 %). Cr mainly comes from industrial production processes, such as steel production and fuel burning (Liu et al., 2018a), while Zn, Mn and Fe are mainly derived from sintering in iron and steel industries (Cui et al., 2020b; Duan and Tan, 2013). Tian et al. (Tian et al., 2015) indicated that the steel production industry can emit a large amount of Zn (about 60 % in China). Therefore, factor 4 can be assigned as iron and steel industry source, which was an important source of elements in $PM_{2.5}$ at Changzhou, accounting for the highest proportion (32.0 %) of the total element mass.

Factor 5 was characterized by Si, Ti and Ca, with relative contributions to the total analyzed elements mass of 78.8 %, 87.5 %, and 68.0 %, respectively. Generally, Si, Ti and Ca are mainly emitted from minerals powder, construction dust, traffic emissions and soil of industry (Gao et al., 2016; Rai et al., 2020b). Si and Ca, as the two most abundant elements in the upper crust, are mainly derived from wind-blown dust in atmosphere (Chang et al., 2018). The correlation analysis of Si, Ti and Ca ($R \geq 0.75$, $P < 0.01$, Fig. S5) also showed that these three elements have the same sources. Therefore, factor 5 can be considered as soil dust, accounting for 23.5 % of the total PM elements at Changzhou.

Factor 6 is related with fireworks, characterized by high K (65.3 %), V (53.0 %), Ba (83.2 %) and Cu (18.2 %). High contents of K, V, Ba and Cu are related to fireworks and firecrackers burning (Kong et al., 2015; Tian et al., 2014). For examples, Cu and Ba elements are often used for manufacturing blue and green fireworks (Rai et al., 2020b). K can be used as an important component of black power in the burning of fireworks and firecrackers (Drewnick et al., 2006). The temporal variations of these elements (Fig. 2) also showed higher concentrations during the CNY. In addition, the diurnal variation of K, V, Ba and Cu was higher at night (19:00–23:00), which was related to the firework events (Fig. 3). Furthermore, the correlation analysis of K, V and Ba ($R \geq 0.86$, $P < 0.01$, Fig. S5) also indicated that these three elements have the same source. The fireworks source explained 14.0 % of the total element sources.

Factor 7 had high loadings of Ni (72.2 %). Ni is an indicator of oil combustion, which can be derived from the heavy oil combustion, lubricating oil and petrochemical (Cheng et al., 2022; Lin et al., 2015; Zhao et al., 2021). By the end of 2019, Changzhou had 32 production berths, and over 50 million tons of goods were transported in the whole year according to the Department of transport of the Jiangsu Province (DTJP, 2020). Therefore, factor 7 was identified as a source related with shipping, which accounted for 0.31 % of the total element sources in this study.

Both results of EFs and PMF showed that Ti and Ca were mainly derived from crustal sources, and other elements were mainly affected by anthropogenic emissions, such as secondary sulfate, fossil fuel combustion, fireworks, traffic emissions and industry.

3.4. Concentrations and source contributions of elements in different periods

The concentrations of elemental compositions and their relative abundances to total element mass during different periods are shown in Fig. 6. The higher contributions of S to mass elements were observed during P1 (47.4 %), P6 (57.1 %), P7 (55.0 %) and P9 (45.6 %), which suggested that those periods were possibly affected by secondary sulfate. Previous surveys indicated that S can be emitted either from the combustion of coal or from the photoreaction of secondary sulfate (Zhang et al., 2018). This was recognized by PMF modeling results in Section 3.3.2. Backward trajectories, source concentrations (seven factors) and hourly source analysis during different periods are shown in Fig. S7, Fig. S8 and Fig. S9a-k. As

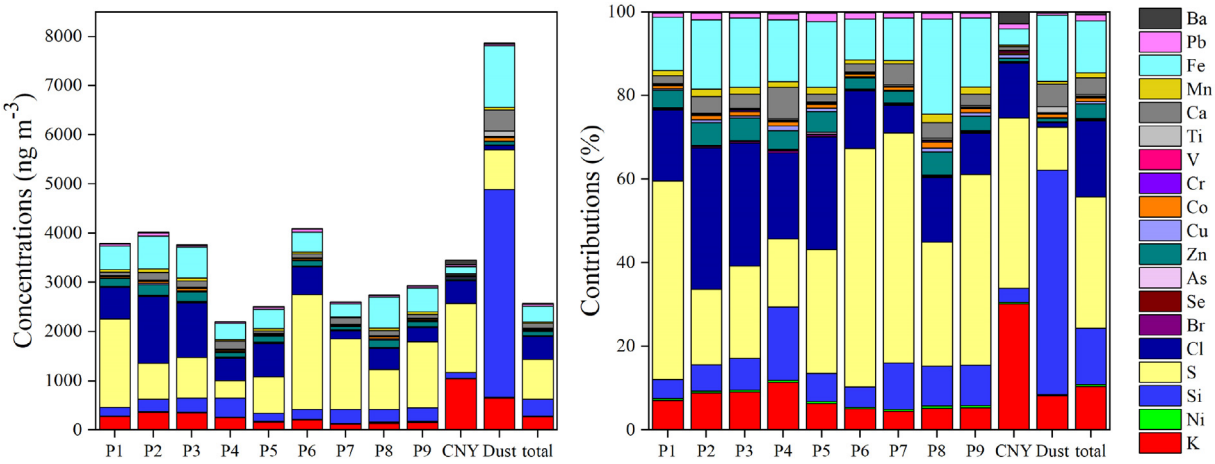

Fig. 6. Concentrations of elemental compositions and their relative contributions to total elements.

shown in Fig. S8, the higher contributions of secondary sulfate mixed with coal combustion to elements mass were also observed during the P1 (26.8 %), P6 (27.1 %) P7 (38.4 %) and P9 (27.8 %), mainly due to the aging of aerosol and coal combustion from Shandong, Jiangsu, southern areas of China (such as Shanghai, and Anhui, Zhejiang, Jiangxi Provinces) and the ocean (Fig. S7). Compared with other pollution periods, the proportion of Cl was the highest in the P2-P5 (Fig. 6), with relative contributions of 33.8 %, 29.4 % 20.6 % and 27.0 %, respectively. Fig. S8 also exhibited that the contributions of Cl-rich aerosol are high during P2-P5, accounting for 13.3 %, 9.1 %, 9.5 % and 7.8 %, respectively. This phenomenon suggests that P2-P5 may be affected by coal/garbage combustion and biomass burning. The air masses of P4 and P5 were mainly influenced by southern areas of China (such as Anhui, Zhejiang and Jiangxi provinces). The contributions of Cu and Pb were higher in P2, P4 and P5 compared with other periods (Fig. 6), and the contributions of traffic also increased during the P2 (7.3 %), P4 (7.9 %) and P5 (9.8 %). Overall, iron and steel industry exhibited higher contributions during P1-P3, P5, P6, P8 and P9, with the relative contributions of 44.3 %, 48.6 %, 48.3 %, 46.5 %, 43.3 %, 58.5 % and 40.7 %, respectively, which suggested that those periods at Changzhou were mainly affected by iron and steel industry. Moreover, the hourly source analysis results further confirmed that the iron and steel source was the main pollution source of P1-P3, P5, P6, P8 and P9 during the observation period (Fig. S9). Based on the analysis of 48 h backward trajectory (Fig. S7), the air masses in P1-P3 periods were mainly derived from western Inner Mongolia, Shanxi, Hebei, Shandong, Anhui, and Jiangsu Province, most of which are the polluted and heavily populated areas of China. In addition, the air mass of P8 was affected by short-distance transmission and was dominated by the local steel industrial sources (58.5 %). The contributions of Si (17.6 %) and Ca (7.5 %) increased significantly in P4 compared with other pollution periods, and the contributions of soil dust also increased by 28.8 % in P4 based on PMF, which were mainly affected by the transmission of northwest and southwest air masses.

Concentration of K increased significantly in CNY (11 February-17 February 2021), and the contributions of Cu, Ba and V also increased significantly compared with other pollution periods. Fireworks can release large amounts of K, Cu, V and Ba (Cui et al., 2020a; Kong et al., 2015; Yu et al., 2019). Moreover, the relative contributions of Ni, Br, As, Zn, Co, Cr, Ca, Mn and Fe decreased during the CNY (Fig. 7), which were mainly attributable to the suspension of production by companies and factories to celebrate the Spring Festive. The air masses of CNY were mainly derived from northern China and northern Zhejiang province. The concentration of $PM_{2.5}$ showed a correlation ($0.20 \leq R \leq 0.35$, $P < 0.05$, Table S5) with fireworks tracers (K, V, Ba, and Cu), suggesting that $PM_{2.5}$ can reflect the influence of firework. There is no strong correlation ($R \leq 0.13$, $P > 0.1$, Table S5) between SO_2 and firework tracers (K, V and Ba) during the Chinese New Year (CNY), suggesting that SO_2 may be dominantly affected by loose coal combustion and long-distance transmission. As shown in Fig. S8 and Fig.S9, the results of the total contribution of fireworks

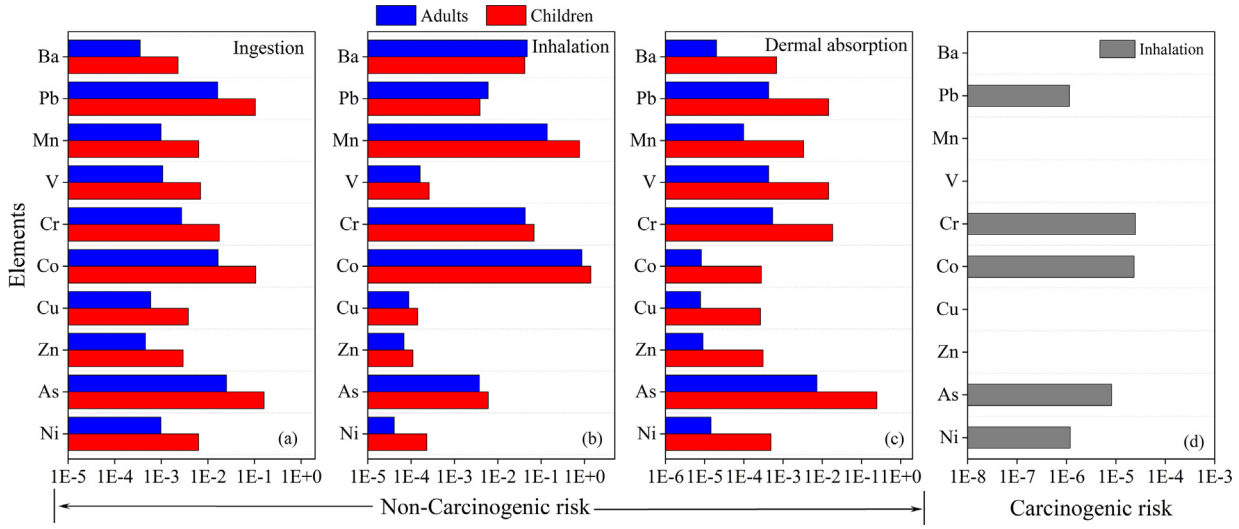

Fig. 7. Risk values of noncarcinogenic risk (a, b, c) and carcinogenic risk (d) in different elements in Changzhou.

(65.5 %) and hourly source analysis showed that the CNY period was mainly affected by the release of fireworks. Therefore, the above results indicated that fireworks and firecrackers were the primary source of $PM_{2.5}$ elements during the CNY at Changzhou.

The contributions of Si, Fe, Ca and Ti were the main contribution species in the Dust period, which was mainly influenced by ocean and northern air masses (Fig. S7), and the results of soil dust contribution (75.3 %) and hourly source analysis indicated that soil dust was the main source during the Dust period (Fig. S8 and Fig. S9 k). Furthermore, we found a strong correlation between PM_{10} and dust tracers during the Dust period ($R \geq 0.78$, $P < 0.01$, Table S6), indicating that PM_{10} can reflect the influence from dust.

3.5. Health risk assessments of $PM_{2.5}$-bound elements in Changzhou

The estimated values of noncarcinogenic risk (NCR) and carcinogenic risk (CR) are presented in Fig. 7. There is an obvious health risk of NCR effect when the HQ or HI value >1. The acceptable risk of CR is $<1 \times 10^{-6}$ (Cui et al., 2020a). As shown in Fig. 6 and Table S7, the NCR values of $PM_{2.5}$-bound metals was evaluated through ingestion, inhalation, and dermal absorption routes for children (adults) were 0.42 (0.07), 2.29 (1.11) and 0.30 (0.01), respectively. According to our results, Co was the dominant species to $NCR_{children}$ by inhalation routes and its HQ value (1.40) was higher than 1, indicating an adverse NCR for children. Most of the individual HQ values in this study was lower than 1, suggesting no obvious non-carcinogenic influence, while the total HI (sum of the HQ) value via inhalation routes was 2.29 for children and 1.11 for adults, respectively, which was beyond the safe value (HQ = 1), indicating the obvious risk of non-carcinogenic effects in Changzhou. As was the dominant species to NCR through ingestion and dermal absorption routes with HQ values below 1. The total NCR for children (3.01) was about 2.5 times higher than that of adults (1.18), indicating more non-carcinogenic influence from metals on children. Co (50.1 %), Mn (25.6 %) and As (13.8 %) were the dominant species contributing to $NCR_{children}$, and Co (75 %), Mn (11.7 %) and Cr (3.9 %) were the major species contributing to NCR_{adults}.

For carcinogenic elements, the total CR in Changzhou was 5.87×10^{-5}, significantly higher than the acceptable (1×10^{-6}) risk levels, suggesting that there is a potential carcinogenic risk during the sampling period. Compared to other cities, the total CR value was lower than Beijing (1.1×10^{-2}) (Cui et al., 2020a), Foshan (3.37×10^{-3}) (Zhou et al., 2018), and Taiyuan ($>1 \times 10^{-4}$) (Liu and Ren, 2019), but higher than Huanggang (10^{-14}–10^{-12}) (Li et al., 2021) and Zhuhai (10^{-6}–10^{-5}) (Yang et al., 2019), indicating that there is a certain level of carcinogenic risk in Changzhou. The CR of each carcinogenic element were ranked in the following order: Cr (2.48×10^{-5}) > Co (2.34×10^{-5}) > As (8.20×10^{-6}) > Ni (1.19×10^{-6}) > Pb (1.15×10^{-6}). Among the CR elements, Cr, Co and As were found to be the dominant risk species, which contributed 42 %, 40 % and 14 % to the total CR, respectively. Those results indicated that the control of Cr, Co and As emissions is important to decrease the carcinogenic risk in Changzhou.

4. Conclusions

The hourly time-resolved trace elements in $PM_{2.5}$ were observed at an urban site in Changzhou from December 10, 2020 to March 31, 2021. Results indicate relatively high $PM_{2.5}$ pollutions with the maximum hourly mean concentration over 140 μg m^{-3} in winter in Changzhou. S, Cl, Si and Fe were the dominant elements in the whole period with an average mass concentrations exceeding 300 ng m^{-3}. The diurnal variations of elements in $PM_{2.5}$ reflected comprehensive impacts from various emission sources as well as the changes in meteorological circumstances (e.g., PBL). EFs analysis showed that the majority of elements were mainly derived from human activities. Seven sources for elements (secondary sulfate mixed with coal combustion, Cl-rich, traffic, iron and steel industry, soil dust, fireworks, and shipping) in $PM_{2.5}$ were recognized by PMF model based on the hourly elemental data. Iron and steel industry source was the largest contributor to $PM_{2.5}$ elemental mass (together accounting for 32.0 %), followed by soil dust (23.5 %). Notably, results from EFs and PMF were similar, indicating that the elements at Changzhou were mainly influenced by anthropogenic emissions. Health risk assessment results suggested that the CR values of Cr and Co were much greater than the admissible levels (1×10^{-6}). Controlling industrial emissions could be of great significance for reducing carcinogenic risk in Changzhou. Collectively, our study provides insights into sources of elements in $PM_{2.5}$, guiding effective control strategies for reducing emissions and health risks of elements in the YRD region.

Author contribution

LL formulated the research objectives, edited and reviewed the manuscript. YNY and KZ conducted the data analyzes and wrote the manuscript with assistance from all co-authors. KZ, QL, RL, LMY, ZQL and XJZ contributed to field observations. SYW, HC, LH and YJW contributed to data analysis and discussions. LL, JZY, and KZ reviewed and modified the manuscript. Data were explained and discussed by all authors.

Data availability

Data will be made available on request.

Declaration of competing interest

The authors declare that they have no conflict of interest.

Acknowledgement

This study is financially supported by the National Natural Science Foundation of China (NO. 41875161, 42075144) and Changzhou Ecological and Environmental Bureau. We thank colleagues at Jiangsu Changzhou Environmental Monitoring Center for help settling the field measurement.

Appendix A. Supplementary data

Supplementary data to this article can be found online at https://doi.org/10.1016/j.scitotenv.2022.158450.

References

Alharbi, B.H., Pasha, M.J., Al Shamsi, S.M.A., 2019. Influence of different urban structures on metal contamination in two metropolitan cities. Sci. Rep. 9, 4920. https://doi.org/10.1038/s41598-019-40180-x.

Cao, F., Zhang, Y., Lin, X., Zhang, Y., 2021. Characteristics and source apportionment of non-polar organic compounds in $PM_{2.5}$ from the three megacities in Yangtze River Delta region, China. Atmos. Res., 252 https://doi.org/10.1016/j.atmosres.2020.105443.

Chang, Y., Huang, K., Xie, M., Deng, C., Zou, Z., Liu, S., et al., 2018. First long-term and near real-time measurement of trace elements in China's urban atmosphere: temporal variability, source apportionment and precipitation effect. Atmos. Chem. Phys. 18, 11793–11812. https://doi.org/10.5194/acp-18-11793-2018.

Cheng, K., Chang, Y., Kuang, Y., Khan, R., Zou, Z., 2022. Elucidating the responses of highly time-resolved $PM_{2.5}$ related elements to extreme emission reductions. Environ. Res. 206. https://doi.org/10.1016/j.envres.2021.112624.

Cui, Y., Ji, D., Chen, H., Gao, M., Maenhaut, W., He, J., et al., 2019. Characteristics and sources of hourly trace elements in airborne fine particles in Urban Beijing, China. J. Geophys. Res. Atmos. 124, 11595–11613. https://doi.org/10.1029/2019jd030881.

Cui, Y., Ji, D., He, J., Kong, S., Wang, Y., 2020a. In situ continuous observation of hourly elements in $PM_{2.5}$ in urban Beijing, China: occurrence levels, temporal variation, potential source regions and health risks. Atmos. Environ. 222, 117164. https://doi.org/10.1016/j.atmosenv.2019.117164.

Cui, Y., Ji, D., Maenhaut, W., Gao, W., Zhang, R., Wang, Y., 2020b. Levels and sources of hourly $PM_{2.5}$-related elements during the control period of the COVID-19 pandemic at a rural site between Beijing and Tianjin. Sci. Total Environ. 744, 140840. https://doi.org/10.1016/j.scitotenv.2020.140840.

Deng, Y., Liu, Y., Wang, T., Cheng, H., Feng, Y., Yang, Y., et al., 2020. Photochemical reaction of CO_2 on atmospheric mineral dusts. Atmos. Environ. 223. https://doi.org/10.1016/j.atmosenv.2019.117222.

Drewnick, F., Hings, S.S., Curtius, J., Eerdekens, G., Williams, J., 2006. Measurement of fine particulate and gas-phase species during the New Year's fireworks 2005 in Mainz, Germany. Atmos. Environ. 40, 4316–4327. https://doi.org/10.1016/j.atmosenv.2006.03.040.

DTJP, 2020. Jiangsu traffic overview in 2019 (traffic yearbook). Available online at:Department of transport of the Jiangsu Province. http://jtyst.jiangsu.gov.cn/art/2020/11/2/art_77201_9584110.html.

Duan, J., Tan, J., 2013. Atmospheric heavy metals and arsenic in China: situation, sources and control policies. Atmos. Environ. 74, 93–101. https://doi.org/10.1016/j.atmosenv.2013.03.031.

Ellouz, F., Masmoudi, M., Quisefit, J.P., Medhioub, K., 2013. Characteristics of trace elements in aerosols collected in northern Tunisia. Phys. Chem. Earth A/B/C 55–57, 35–42. https://doi.org/10.1016/j.pce.2010.12.003.

EPA, 2011. Exposure Factors Handbook 2011 Edition (Final Report). U.S. Environmental Protection Agency, Washington, DC EPA/600/R-09/052F.

Fan, M., Zhang, Y., Lin, Y., Cao, F., Sun, Y., Qiu, Y., et al., 2021. Specific sources of health risks induced by metallic elements in $PM_{2.5}$ during the wintertime in Beijing, China. Atmos. Environ. 246. https://doi.org/10.1016/j.atmosenv.2020.118112.

Gani, S., Bhandari, S., Seraj, S., Wang, D.S., Patel, K., Soni, P., et al., 2019. Submicron aerosol composition in the world's most polluted megacity: the Delhi aerosol supersite study. Atmos. Chem. Phys. 19, 6843–6859. https://doi.org/10.5194/acp-19-6843-2019.

Gao, J., Peng, X., Chen, G., Xu, J., Shi, G., Zhang, Y., et al., 2016. Insights into the chemical characterization and sources of $PM_{2.5}$ in Beijing at a 1-h time resolution. Sci. Total Environ. 542, 162–171. https://doi.org/10.1016/j.scitotenv.2015.10.082.

Han, Y., Kim, H., Cho, S., Kim, P., Kim, W., 2015. Metallic elements in $PM_{2.5}$ in different functional areas of Korea: concentrations and source identification. Atmos. Res. 153, 416–428. https://doi.org/10.1016/j.atmosres.2014.10.002.

Huang, J., Zhang, Z., Tao, J., Zhang, L., Nie, F., Fei, L., 2022. Source apportionment of carbonaceous aerosols using hourly data and implications for reducing $PM_{2.5}$ in the Pearl River Delta region of South China. Environ. Res. 210. https://doi.org/10.1016/j.envres.2022.112960.

Jena, S., Singh, G., 2017. Human health risk assessment of airborne trace elements in Dhanbad, India. Atmos. Pollut. Res. 8, 490–502. https://doi.org/10.1016/j.apr.2016.12.003.

Jensen, A., Liu, Z., Tan, W., Dix, B., Chen, T., Koss, A., et al., 2021. Measurements of volatile organic compounds during the COVID-19 lockdown in Changzhou, China. Geophys. Res. Lett. 48. https://doi.org/10.1029/2021GL095560.

Kong, S.F., Li, L., Li, X., Yin, Y., Chen, K., Liu, D.T., et al., 2015. The impacts of firework burning at the chinese spring festival on air quality: insights of tracers, source evolution and aging processes. Atmos. Chem. Phys. 15, 2167–2184. https://doi.org/10.5194/acp-15-2167-2015.

Li, G., Bei, N., Cao, J., Huang, R., Wu, J., Feng, T., et al., 2017. A possible pathway for rapid growth of sulfate during haze days in China. Atmos. Chem. Phys. 17, 3301–3316. https://doi.org/10.5194/acp-17-3301-2017.

Li, R., Wang, Q., He, X., Zhu, S., Zhang, K., Duan, Y., et al., 2020. Source apportionment of $PM_{2.5}$ in Shanghai based on hourly organic molecular markers and other source tracers. Atmos. Chem. Phys. 20, 12047–12061. https://doi.org/10.5194/acp-20-12047-2020.

Li, X., Mao, Y., Chen, Z., Liu, W., Cheng, C., Mingming, Shi, et al., 2021. Characteristics and health risk assessment of heavy metals in $PM_{2.5}$ under winter haze conditions in Central China: a case study of Huanggang, Hubei Province. EnvironmentalScience 42, 4593–4601.

Li, X., Yan, C., Wang, C., Ma, J., Li, W., Liu, J., et al., 2022. $PM_{2.5}$-bound elements in Hebei Province, China: pollution levels, source apportionment and health risks. Sci. Total Environ. 806. https://doi.org/10.1016/j.scitotenv.2021.150440.

Lin, Y.C., Tsai, C.J., Wu, Y.C., Zhang, R., Chi, K.H., Huang, Y.T., et al., 2015. Characteristics of trace metals in traffic-derived particles in hsuehshan tunnel, Taiwan: size distribution, potential source, and fingerprinting metal ratio. Atmos. Chem. Phys. 15, 4117–4130. https://doi.org/10.5194/acp-15-4117-2015.

Liu, K., Ren, J., 2019. Characteristics, sources and health risks of $PM_{2.5}$-bound potentially toxic elements in the northern rural China. AtmosphericPollut. Res. 10, 1621–1626. https://doi.org/10.1016/j.apr.2019.06.002.

Liu, J., Chen, Y., Chao, S., Cao, H., Zhang, A., Yang, Y., 2018. Emission control priority of $PM_{2.5}$-bound heavy metals in different seasons: a comprehensive analysis from health risk perspective. Sci. Total Environ. 644, 20–30. https://doi.org/10.1016/j.scitotenv.2018.06.226.

Liu, J., Gu, Y., Ma, S., Su, Y., Ye, Z., 2018. Day-night differences and source apportionment of inorganic components of $PM_{2.5}$ during summer-winter in Changzhou city. EnvironmentalScience 39, 980–989.

Manisalidis, I., Stavropoulou, E., Stavropoulos, A., Bezirtzoglou, E., 2020. Environmental and health impacts of air pollution: a review. Front. Public Health 8, 14. https://doi.org/10.3389/fpubh.2020.00014.

Manousakas, M., Papaefthymiou, H., Diapouli, E., Migliori, A., Karydas, A., Radovic, I., et al., 2017. Assessment of $PM_{2.5}$ sources and their corresponding level of uncertainty in a coastal urban area using EPA PMF 5.0 enhanced diagnostics. Sci. Total Environ. 574, 155–164. https://doi.org/10.1016/j.scitotenv.2016.09.047.

Ministry of Environmental Protection of the People's Republic of China (MEP), 1990. Background Contents on Elements of Soils in China (in Chinese).

MEP. Ministry of Environmental Protection of the People's Republic of China (MEP), 2019. Technical guidelines for risk assessment of soil contamination of land for construction. https://www.mee.gov.cn/ywgz/fgbz/bz/bzwb/trhj/201912/W020191224560850148092.pdf 2019.

Niu, Y., Wang, F., Liu, S., Zhang, W., 2021. Source analysis of heavy metal elements of $PM_{2.5}$ in canteen in a university in winter. Atmos. Environ. 244, 117879. https://doi.org/10.1016/j.atmosenv.2020.117879.

Paatero, P., Tapper, U., 1994. Positive matrix factorization: a non-negative factor model with optimal utilization of error estimates of data value. Environmetrics 5, 111–126.

Pant, P., Shukla, A., Kohl, S.D., Chow, J.C., Watson, J.G., Harrison, R.M., 2015. Characterization of ambient $PM_{2.5}$ at a pollution hotspot in New Delhi, India and inference of sources. Atmos. Environ. 109, 178–189. https://doi.org/10.1016/j.atmosenv.2015.02.074.

Pope, C., Ezzati, M., Cannon, J., Allen, R., Jerrett, M., Burnett, R., 2018. Mortality risk and $PM_{2.5}$ air pollution in the USA: an analysis of a national prospective cohort. Air Qual Atmos Health 11, 245–252. https://doi.org/10.1007/s11869-017-0535-3.

Rai, P., Furger, M., El Haddad, I., Kumar, V., Wang, L., Singh, A., et al., 2020. Real-time measurement and source apportionment of elements in Delhi's atmosphere. Sci. Total Environ. 742. https://doi.org/10.1016/j.scitotenv.2020.140332.

Rai, P., Furger, M., Slowik, J.G., Canonaco, F., Fröhlich, R., Hüglin, C., et al., 2020. Source apportionment of highly time-resolved elements during a firework episode from a rural freeway site in Switzerland. Atmos. Chem. Phys. 20, 1657–1674. https://doi.org/10.5194/acp-20-1657-2020.

Rai, P., Slowik, J.G., Furger, M., El Haddad, I., Visser, S., Tong, Y., et al., 2021. Highly time-resolved measurements of element concentrations in PM_{10} and $PM_{2.5}$: comparison of Delhi, Beijing, London, and Krakow. Atmospheric Chemistry and Physics 21, 717–730. https://doi.org/10.5194/acp-21-717-2021.

Reizer, M., Calzolai, G., Maciejewska, K., Orza, J.A.G., Carraresi, L., Lucarelli, F., et al., 2021. Measurement report: receptor modeling for source identification of urban fine and coarse particulate matter using hourly elemental composition. Atmos. Chem. Phys. 21, 14471–14492. https://doi.org/10.5194/acp-21-14471-2021.

Sharma, S.K., Mandal, T.K., Saxena, M., Rashmi, Sharma, A., Datta, A., 2014. Variation of OC, EC, WSIC and trace metals of PM_{10} in Delhi, India. J. Atmos. Sol. Terr. Phys. 113, 10–22. https://doi.org/10.1016/j.jastp.2014.02.008.

Shukla, A.K., Lalchandani, V., Bhattu, D., Dave, J.S., Rai, P., Thamban, N.M., et al., 2021. Real-time quantification and source apportionment of fine particulate matter including organics and elements in Delhi during summertime. Atmos. Environ. 261. https://doi.org/10.1016/j.atmosenv.2021.118598.

Tian, Y.Z., Wang, J., Peng, X., Shi, G.L., Feng, Y.C., 2014. Estimation of the direct and indirect impacts of fireworks on the physicochemical characteristics of atmospheric PM_{10} and $PM_{2.5}$. Atmos. Chem. Phys. 14, 9469–9479. https://doi.org/10.5194/acp-14-9469-2014.

Tian, H.Z., Zhu, C.Y., Gao, J.J., Cheng, K., Hao, J.M., Wang, K., et al., 2015. Quantitative assessment of atmospheric emissions of toxic heavy metals from anthropogenic sources in China: historical trend, spatial distribution, uncertainties, and control policies. Atmos. Chem. Phys. 15, 10127–10147. https://doi.org/10.5194/acp-15-10127-2015.

Wang, Q., Dai, X., Ke, W., Shang, T., 2015. Analysis and pollution characteristics of metal elements in $PM_{2.5}$ in Changzhou during spring. Chin. J. Environ. Eng. 9, 323–330.

Wang, Y., Jia, C., Tao, J., Zhang, L., Liang, X., Ma, J., et al., 2016. Chemical characterization and source apportionment of $PM_{2.5}$ in a semi-arid and petrochemical-industrialized city, Northwest China. Sci. Total Environ. 573, 1031–1040. https://doi.org/10.1016/j.scitotenv.2016.08.179.

Wang, S., Hu, G., Yu, R., Shen, H., Yan, Y., 2021. Bioaccessibility and source-specific health risk of heavy metals in $PM_{2.5}$ in a coastal city in China. Environ. Adv. 4. https://doi.org/10.1016/j.envadv.2021.100047.

Wang, W., Liu, M., Wang, T., Song, Y., Zhou, L., Cao, J., et al., 2021. Sulfate formation is dominated by manganese-catalyzed oxidation of SO_2 on aerosol surfaces during haze events. Nat. Commun. 12, 1993. https://doi.org/10.1038/s41467-021-22091-6.

WHO, 2021. Global air quality guidelines. Particulate matter ($PM_{2.5}$ and PM_{10}), ozone, nitrogen dioxide, sulfur dioxide and carbon monoxide. Executive summary. World Health Organization, Geneva. https://www.who.int/publications/i/item/9789240034433.

WHO, 2022. Air pollution. WHO. Available online at: https://www.who.int/airpollution/en/. (Accessed 16 March 2022).

Xu, P., Chen, Y.S., He, S., Chen, W., Wu, L., Xu, D., et al., 2019. A follow-up study on the characterization and health risk assessment of heavy metals in ambient air particles emitted from a municipal waste incinerator in Zhejiang, China. Chemosphere 246, 125777.

Yan, R.H., Peng, X., Lin, W., He, L.Y., Wei, F.H., Tang, M.X., 2022. Trends and challenges regarding the source-specific health risk of $PM_{2.5}$-bound metals in a Chinese Megacity from 2014 to 2020. Environ. Sci. Technol. 56, 6996–7005. https://doi.org/10.1021/acs.est.1c06948.

Yang, Y., Jia, Y., Bian, G., Yu, X., Zhong, C., Quan, D., 2019. Elemental characteristics and health risk assessment of heavy metals in atmospheric $PM_{2.5}$ in a suburb of Zhuhai city. Environ. Sci. 40, 1553–1561.

Yu, Y., He, S., Wu, X., Zhang, C., Yao, Y., Liao, H., et al., 2019. $PM_{2.5}$ elements at an urban site in Yangtze River Delta, China: high time-resolved measurement and the application in source apportionment. Environ. Pollut. 253, 1089–1099. https://doi.org/10.1016/j.envpol.2019.07.096.

Zhang, Y.L., Cao, F., 2015. Fine particulate matter ($PM_{2.5}$) in China at a city level. Sci. Rep. 5, 14884. https://doi.org/10.1038/srep14884.

Zhang, J., Zhou, X., Wang, Z., Yang, L., Wang, J., Wang, W., 2018. Trace elements in $PM_{2.5}$ in Shandong Province: source identification and health risk assessment. Sci. Total Environ. 621, 558–577. https://doi.org/10.1016/j.scitotenv.2017.11.292.

Zhang, Q., Xue, D., Liu, X., Gong, X., Gao, H., 2019. Process analysis of $PM_{2.5}$ pollution events in a coastal city of China using CMAQ. J. Environ. Sci. 79, 225–238. https://doi.org/10.1016/j.jes.2018.09.007.

Zhao, S., Tian, H., Luo, L., Liu, H., Wu, B., Liu, S., et al., 2021. Temporal variation characteristics and source apportionment of metal elements in $PM_{2.5}$ in urban Beijing during 2018–2019. Environ. Pollut. 268, 115856. https://doi.org/10.1016/j.envpol.2020.115856.

Zheng, N., Liu, J., Wang, Q., Liang, Z., 2010. Health risk assessment of heavy metal exposure to street dust in the zinc smelting district, northeast of China. Sci. Total Environ. 408, 726–733. https://doi.org/10.1016/j.scitotenv.2009.10.075.

Zhou, S., Davy, P.K., Huang, M., Duan, J., Wang, X., Fan, Q., et al., 2018. High-resolution sampling and analysis of ambient particulate matter in the Pearl River Delta region of southern China: source apportionment and health risk implications. Atmos. Chem. Phys. 18, 2049–2064. https://doi.org/10.5194/acp-18-2049-2018.